Stimulated Brillouin scattering off nonlinear ion acoustic waves

S. Hüller[a)]
Theoretische Quantenelektronik, Institut für Angewandte Physik, Technische Hochschule, D-6100 Darmstadt, Germany

(Received 9 May 1991; accepted 12 August 1991)

The influence of nonlinear ion acoustic waves on the stimulated Brillouin backscattering process is investigated with the help of the hydrodynamic description of the ion fluid. Numerical calculations were systematically performed for a wide range of relevant parameters in the presence of an ideal plasma. It is shown that the scaling of steady-state solutions due to spatially amplified scattering deviates significantly from the theory where only linearized ion acoustic waves are considered. An analytic approach using harmonic expansion confirms the similarity parameters found numerically. The significance of kinetic effects, such as anomalous heat transport due to fast ions and ion trapping in the presence of weakly damped ion waves, is also studied using particle simulations.

I. INTRODUCTION

The description of resonant wave–wave interaction with the use of the equations for the slowly varying complex envelopes (SVE) of the coupled wave components is rather universal for parametric processes.

Scattering of electromagnetic radiation on periodic modulations of the refractive index due to electrostatic or acoustic waves in the medium usually is treated as a three-wave interaction process. Most of the theoretical investigations of stimulated scattering are based on the equations for the wave envelopes. They take into account the dominating nonlinear coupling terms in which the mutual influence of the waves under consideration results in a change of their amplitudes and their phases.

In the approximation of slowly varying envelopes, each wave is assumed to keep its initial shape as a linear wave would. Since this method makes use of the linear dispersion relations in order to eliminate the rapid oscillations in space and time, the phase of any wave is not allowed to depend on the respective amplitude. However, it is well known from nonlinear waves that the deformation of an initially sinusoidal shape is a result of the dependence of the propagation velocity on the local amplitude. An excellent example in the context of stimulated Brillouin scattering (SBS) can be given by the equation for a simple wave representing a freely propagating (ion) acoustic wave[1-3]

$$\frac{\partial v}{\partial t}+[s(v)+v]\frac{\partial v}{\partial x}=0, \tag{1}$$

where s stands for the sound speed and v for the velocity perturbation. For an initial wave profile $v(x,0)$, adjacent fluid elements α and β with $v(x_\alpha)\neq v(x_\beta)$ propagate along different characteristics. This results in the formation of shocklike structures in the wave profile and in wave breaking, which may be regulated and prevented by dispersive and dissipative effects. Although this is a long-time-scale effect, it can cause considerable reduction of the average backscattering level, as long as the excitation due to SBS is not diminished by incoherency. The influence of nonlinear ion sound wave propagation on SBS is the subject of this paper. The importance of incoherent and nonstationary behavior is considered in other papers.[4]

In previous publications,[5-7] nonlinear features of ion acoustic waves (IAW) were included by an extension of the system of coupled equations for the envelopes with a finite number of excited harmonics. In these and in further papers,[8,9] it was shown that the scaling of the parameters determining the level of backscattering deviates from the standard theory[10-12] when IAW nonlinearities or only additional nonlinear terms[8] are taken into account. In contrast to the standard approach where only a linear IAW is assumed, the analytic solutions found in Refs. 5 and 6 are based on a particular balance of the energy flow between the fundamental IAW and its second harmonic, but disregarding linear dissipative terms.

Although harmonic generation is a well-known effect connected with nonlinear waves, the commonly used expansion becomes erroneous if the equation for the considered wave does not completely fulfill a simple wave equation (1), even if the deviation is small. This will be shown in Appendix A.

In the current paper, an extended model is used that intrinsically takes into account all harmonics of the IAW. The results are obtained by solving the full set of the nonlinear hydrodynamic equations of the ion fluid so that an unsatisfactory treatment of SBS by an incomplete system of $3+n$ wave-envelope equations (one fundamental IAW resonant with two electromagnetic wave contributions and n ion acoustic daughter waves) is avoided.

The dependence of the SBS level on the governing parameters, as the incident laser intensity, is elaborated with particular emphasis on the parameter scaling. It will be shown that only for low laser intensities, the result from standard theory can be reproduced, which yields a scaling with a single similarity parameter for the case of spatial amplification.[10-12] We show that, beyond this regime, the simple scaling no longer holds, the parameter dependence splits, and the corresponding solutions lead to reduced backscattering.

[a)]Present address: Max-Planck-Institut für Quantenoptik, D-8046 Garching, Germany.

 0899-8213/91/123317-14$02.00

Although the decomposition of the electromagnetic field into two spectrally well-separated components proves to be a satisfactory approximation in homogeneous media, we still use the original wave equation after the elimination of the high-frequency time dependence. This is advantageous since the full spatial dependence is maintained. Therefore even inhomogeneous profiles with such domains can be treated where the WKB (Wentzel–Kramers–Brillouin) approximation is no longer applicable.

In addition to the hydrodynamic calculations and with the aim to study the influence of nonlinear kinetic effects on the evolution of the IAW, particle-in-cell (PIC) simulations are performed. This approach also covers the domain of weakly damped IAW's, which cannot be adequately treated by a fluid description. The ions are represented by an ensemble of individual "one-dimensional" (1-D) particles. In contrast to previous simulation models,[13] we assume that the electrons, because of their high thermal conduction, form an almost isothermal background. This reduces the numerical expense considerably.

The paper is organized in the following way. In Sec. II, we present the extended model that describes the stimulated backscattering off nonlinear ion sound waves more adequately than the standard system of linearized equations for the wave envelopes. In addition, we reduce the coupled 1-D hydrodynamic equations of the ion fluid to a "quasisimple" wave equation.[14] This enables a facilitated approach to the analytic determination of the steady-state solutions in presence of ion acoustic nonlinearities. Section III is concerned with numerical solutions of the extended model. The dynamic evolution will be discussed and illustrated. The scaling of the parameters for asymptotically attained steady-state solutions will be pointed out in Sec. IV. A path to obtain the scaling of the steady-state problem analytically is sketched. From this, we derive the solution in lowest order of the approximation that already yields a scaling to a comparable combination of similarity parameters as obtained from the numerical calculations. In Sec. V, we discuss the results from PIC-code simulations of SBS.

II. THE NONLINEAR MODEL

The mutual interaction of electromagnetic radiation and almost-neutral density fluctuations due to acoustic waves requires a polarizability of the (quasineutral) medium. Of course, this is guaranteed in ideal plasmas, which are the only media considered in this work. The action of the ponderomotive force of the electromagnetic (or electron-plasma) wave on the long-time-scale motion of the electrons is then transferred to the ion fluid. This can be expressed with the help of the 1-D hydrodynamic equations, written here in quantities that are already normalized with respect to the IAW fluid,

$$\frac{dn_i}{dt}+n_i\frac{\partial v}{\partial x}=0, \tag{2a}$$

$$\frac{dv}{dt}+\frac{1}{n_0}\frac{\partial p}{\partial x}=-Z\frac{\partial \Phi}{\partial x}+\mu\frac{\partial^2 v}{\partial x^2}-\nu v. \tag{2b}$$

Here, m_i, n_i, Z, and v represent the ion mass, ion density, ion charge number, and speed, respectively, ω_a and k_a are the frequency and the wave number of the IAW, and ϕ is the electrostatic potential. In an unnormalized presentation, the quantities in Eqs. (2) have to be replaced by $x \to k_a x$, $t \to \omega_a t$, $v \to v/s$, $\phi \to e\phi/(k_B T_e)$, $\nu \to \nu/\omega_a$, $\mu \to \mu k_a^2/\omega_a$, and $p \to n_i k_B T_i/(m_i s^2)$, using $s^2 = k_B T_e/m_i$ with k_B as the Boltzmann constant and T_i, T_e as the ion and electron temperatures. The ion pressure p can either be eliminated by an equation of state or be determined by introducing an additional energy (or entropy) equation. The coefficient ν phenomenologically represents any linear damping. The dynamical coefficient $\mu\{=\rho^{-1}[(4/3)\eta+\xi+\kappa(c_V^{-1}-c_p^{-1})]\}$ contains all viscous effects (coefficients η and ξ), but also the dissipation by heat conduction (coefficient κ, specific heat c_V, c_p) assuming that adiabaticity ($p \sim n^\gamma$) is only slightly invalidated[14] (as in weak shocks) and the heating itself is negligible, i.e., we assume $T_e, T_i = \text{const}$.

The high-frequency motion of the electrons results in a time-averaged nonlinear force, even in the time scale longer than the ion oscillations, and thus acts on the whole fluid. The corresponding ponderomotive potential Φ_p can be determined from the solution of the electromagnetic (em) wave equation in the medium. This is because the electron oscillatory velocity v_{osc} is in first order proportional to the electric field of the em wave. Thus, for Φ_p, results

$$\Phi_p=(m_e/2k_B T_e)\langle v_{osc}^2\rangle \approx (e^2/2m_e\omega_0^2 k_B T_e)\langle E^2\rangle. \tag{3}$$

In the absence of charge separation, i.e., λ_D (Debye length) $= 0$, $n_e = Zn_i$, Φ is given by the ponderomotive potential and electron pressure. In any other case, where $\lambda_D \neq 0$, the electrostatic potential must be calculated from Poisson's equation where the electron density n_e has to be evaluated from an assumed quasistatic electron motion. This assumption leads to a Boltzmann factor where the ponderomotive potential appears in the exponent similar to a chemical potential,

$$n_e=n_0 e^{(\Phi-\Phi_p-v_{dc}^2/2)}. \tag{4}$$

The v_{dc}^2 term arises from the assumption of irrotational flow ($\nabla\times\mathbf{v}_{dc}=0$) and is due to any dc current appearing as $(\mathbf{v}_{dc}\cdot\nabla)\mathbf{v}_{dc}$ in the electron momentum equation. This term will be disregarded for simplicity. Hence the Poisson equation becomes the nonlinear expression

$$\frac{\partial^2\Phi}{\partial x^2}=\frac{1}{(k_a\lambda_D)^2}\frac{n_e-Zn_i}{n_0}=\frac{1}{(k_a\lambda_D)^2}\left(e^{\Phi-\Phi_p}-\frac{Zn_i}{n_0}\right). \tag{5}$$

For small λ_D compared with the wavelength $\lambda_a = 2\pi/k_a$, i.e., $(k_a\lambda_D)^2 \ll 1$, Eq. (4) can be written in an iterative operational form as

$$\Phi\approx\left(1+(k_a\lambda_D)^2\frac{\partial^2}{\partial x^2}\right)\left(\Phi_p-\ln\frac{Zn_i}{n_e}\right), \tag{6}$$

where $(k_a\lambda_D)^2\partial_{xx}(\ldots)$ leads to a dispersive term in Eq. (2b), equivalent to $\partial^3 v/\partial x^3$ in the Korteweg–de Vries equation.

The density perturbations originating from the sound wave and the ponderomotive force action take place over a much longer time scale than the laser light period. This allows the usual reduction of the time derivatives of the envelopes of $\mathbf{E}$ and the current density $\mathbf{j}$ in the em wave equation, with $\mathbf{E} = \mathbf{e}_\perp\, Ee^{-i\omega_0 t}$, $\mathbf{j} = \mathbf{e}_\perp\, je^{-i\omega_0 t}$, $\mathbf{e}_\perp \perp \mathbf{e}_k = \mathbf{k}/k$, as well as Ohm's law. Using $n(x,t) = n_e \approx Zn_i$, one obtains

$$\frac{\partial j}{\partial t} \approx -i\omega_0 j \approx -\frac{n(x,t)e^2}{m_e}\left(1 + i\frac{\nu_{ei}}{\omega_0}\right)^{-1} E,$$

where ν_{ei} denotes the absorption coefficient due to inverse Bremsstrahlung. The resulting em wave equation, which still includes the high-frequency oscillations in space, can be written as

$$\frac{i}{2}\frac{\omega_a}{\omega_0}\frac{\partial E}{\partial t} + \frac{\partial^2 E}{\partial x^2} + \frac{1}{4\epsilon}\left[1 - \frac{n(x,t)}{n_c}\left(1 + i\frac{\nu_{ei}}{\omega_0}\right)^{-1}\right]E = 0. \tag{7}$$

It completes the system of model equations. Herein we used $\nabla \cdot \mathbf{E} = 0$, the definition of the critical density $n_c = e^2/(\epsilon_0 m_e \omega_0^2)$, $\epsilon = 1 - n_0/n_c$, as well as the relation between the acoustic and em wave numbers, $k_a \approx 2k_0 \approx 2\epsilon^{1/2}\omega_0/c$. This last condition is necessary for Brillouin backscattering because of the small frequency ratio, $\omega_a/\omega_0 \ll 1$. This homogeneous partial differential equation (7) is quasilinear since its coefficients depend on x and t, and remains unchanged after normalization with respect to the incoming electric field $\hat{E} = E(x = 0)$.

The hydrodynamic part [Eqs. (2)] of the complete system of equations (2), (3), (5), and (6) can be simplified by the assumption that the behavior of the density $\rho = m_i n_i$ and pressure $p = p_0(\rho/\rho_0)^\gamma$ deviate only slightly from that of a simple wave. The density of an ideal simple wave $\hat{\rho}$, as all other quantities describing the wave, can be expressed as a function of only one of them, for example as a function of v, i.e., $\hat{\rho} = \hat{\rho}(v)$ and $p = p(v)$. This results in the differential

$$d\hat{\rho} = u^2\left(\frac{d\hat{\rho}}{dv}\right)dv,$$

where u stands for the normalized speed of sound, defined by $u^2 = d(p_e + p_i)/d\hat{\rho} = 1 + \gamma_i T_i/(ZT_e)$. The correct density $\rho(x,t)$, however, consists of $\hat{\rho}(v)$ and a small perturbation $\psi(\ll\hat{\rho})$ explicitly depending on x and t,

$$\rho(x,t) = \hat{\rho}(v) + \psi(x,t).$$

The resulting equation (see Appendix A) for "quasisimple" waves

$$\frac{\partial v}{\partial t} + [u(v) + v]\frac{\partial v}{\partial x} = \frac{1}{2}\left(\mu\frac{\partial^2 v}{\partial x^2} - \frac{\partial \Phi_p}{\partial x}\right) + \mathbf{O}(\psi^2), \tag{8}$$

is the basis for a harmonic expansion of the IAW.[5–7] Starting from the fundamental ($m = 1$) IAW component w_1, the differential equation for the nth harmonic w_n reads (using $u \approx 1$)

$$\frac{\partial w_n}{\partial t} + \frac{\partial w_n}{\partial x} + \nu_n w_n = \frac{1}{2}\varphi_p \delta_{n,1} - \frac{n}{2}\left(\sum_{m<n} w_m w_{n-m} - 2\sum_m w_m w_{m+n}\right). \tag{9}$$

This equation contains a wave-number-dependent damping $\nu_n = \nu(n)$, as well as the ansatz $v(x,t) = \Sigma_m v_m = \Sigma_m w_m \sin m(x - t)$. Furthermore, it is sufficient to assume a single-harmonic contribution for the ponderomotive potential $\Phi_p = \varphi_p \cos(x - t)$. The symbol $\delta_{n,1}$ denotes the Kronecker delta. Besides the coupling between IAW and the ponderomotive force of the em waves, defined by (using $\xi = x - t$),

$$-\left\langle v\frac{\partial \Phi_p}{\partial x}\right\rangle := \int_0^{2\pi} v(\xi)\varphi_p \sin\xi\, d\xi = \frac{1}{2}\sum_m \varphi_p w_m \delta_{m,1} = \frac{1}{2}\varphi_p w_1,$$

the interaction of the harmonic contributions causes additional nonlinear terms [on the right-hand side (rhs)] in the energy balance

$$\sum_m \left(\frac{\partial w_m^2}{\partial t} + \frac{\partial w_m^2}{\partial x} + 2\nu_m w_m^2\right) + 2\left\langle v_1\frac{\partial \Phi_p}{\partial x}\right\rangle = \sum_m \left(2\sum_n w_m w_n w_{m+n} - \sum_{m<n} w_m w_n w_{m-n}\right). \tag{10}$$

It is obvious that merely the fundamental wave component, which is the only one considered in linearized theory,[15] can interact resonantly with the em waves. Any other harmonic ($n\omega_a \approx nsk_a$) cannot simultaneously fulfill the SBS matching conditions for frequency ω and wave vector $\mathbf{k}$ with the nth harmonic

$$n\omega_a \approx \omega_0 - \omega_i^{(n)} \ll \omega_0$$

and

$$|n\mathbf{k}_a| = |\mathbf{k}_0 - \mathbf{k}_1^{(n)}|,$$

because $\omega_1^{(n)} < \omega_0$ and $|\mathbf{k}_1^{(n)}| \geqslant |n\mathbf{k}_a| - |\mathbf{k}_0| \approx (2n - 1)|\mathbf{k}_0|$ contradict for $n > 1$. The subscript 0 represents the incident em wave, whereas 1 represents the (back)-scattered em wave components for which $\omega_1^{(n)}$ and $\mathbf{k}_1^{(n)}$ correspond to the respective harmonic IAW.

This harmonic expansion is helpful in understanding the mutual interaction in the frame of second quantization. The dynamics of the amplitude can be interpreted by an exchange between photons and phonons in case of SBS, or between phonons and phonons in case of harmonic excitation. [The interaction circuit belonging to the process described above is illustrated in Fig. 1, where a_0 and a_1 stand for the incident and (back-)scattered em wave components, respectively.] On the other hand, one should keep in mind that the expansion due to Eq. (8) up to a certain harmonic ($m \geqslant 2$) becomes erroneous when the amplitude of this daughter wave has values below the accuracy of Eq.

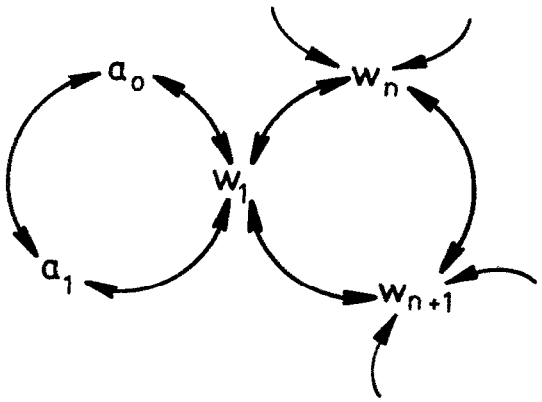

FIG. 1. Circuits describing the interaction between ion acoustic waves and electromagnetic waves. The left circuit represents the resonant coupling between the incident electromagnetic wave ("pump wave") a_0, the backscattered wave a_1, and the fundamental IAW w_1 due to SBS. The interaction between the IAW harmonics w_n (right circuit) is connected to the SBS process only via the fundamental IAW w_1.

(8). In Appendix A, the error caused by the limited accuracy is evaluated for the steady-state case in the wave frame. It essentially leads to dispersion of the wave.

Therefore it is neither reasonable to include high-harmonic contributions into a system of model equations nor to break off after a limited number (m) of daughter waves, i.e., $w_{n>m}=0$.

For this reason, we only use the harmonic expansion in order to find analytically the scaling parameters of the solutions. We shall see later that this will confirm principally the numerically determined scaling behavior. But, for the numerical investigations themselves, we still use the primary hydrodynamic equations (2).

III. NUMERICAL SOLUTION

A. Model equations and parameters

For the purpose of numerical investigations, the hydrodynamic equations are written in Lagrangian coordinates[16,17]

$$x_\alpha(t)=X_\alpha+\int v_\alpha\,dt,$$

where (x_α, v_α) represent a fluid element α of fixed mass, m_α and $X_\alpha = x_\alpha(t=0)$. Also,

$$\frac{\partial v_\alpha}{\partial t}=-\frac{1}{n_0}\frac{\partial p_i}{\partial x}\bigg|_{x_\alpha}-\frac{\partial \Phi}{\partial x}\bigg|_{x_\alpha}-\nu v_\alpha+\mu\frac{\partial^2 v}{\partial x^2}\bigg|_{x_\alpha}, \tag{11a}$$

$$\frac{\partial x_\alpha}{\partial t}=v_\alpha,\quad Zn_\alpha=n_0\left(\frac{\partial x_\alpha}{\partial X_\alpha}\right)^{-1}, \tag{11b}$$

where we assume an adiabatic law $p_i(n_\alpha) = (n_0T_i/ZT_e)\cdot(n_\alpha/n_i)^{\gamma_i}$ with $\gamma_i=3$, representing a plane wave. Here, T_i denotes the equilibrium ion temperature. Poisson's equation

$$\frac{\partial^2\Phi}{\partial x^2}=\frac{1}{(k_d\lambda_D)^2}\left(e^{\Phi-\Phi_p}-\frac{Zn_i}{n_0}\right), \tag{12}$$

using

$$\Phi_p=\hat{I}\langle E^2\rangle\quad\text{with}\quad\hat{I}=\epsilon_0\hat{E}^2/(4n_ck_BT_e), \tag{13}$$

can be evaluated at x_α, though the Lagrangian grid is not equally spaced[17] and nonstationary with respect to the lab frame. However, it is necessary to determine the mass and charge distribution $n(x,t)$ also in Eulerian coordinates, in order to solve the em wave equation (7) without causing any phase shift in E as a consequence of expanding boundaries.

A similar set of equations was investigated by Candy *et al.* in Ref. 9, but they use an Eulerian scheme to solve the hydrodynamic equations (2). This requires a highly accurate procedure in order to avoid numerical diffusion. We applied the set of equations (7) and (11)–(13) to a trapezoidal density profile, representing a homogeneous plasma of length L between two short linear ramps that avoid considerable reflection by an abrupt transition from vacuum to a finite density n_0. In this geometry, with the neighboring vacuum, we obtain natural boundary conditions and are not forced to assume any hypothetic behavior of the IAW at a fixed location in the plasma. In Ref. 4, we also discuss results of our scheme applied to an inhomogeneous linear density profile going from vacuum to an overdense plasma region.

The equations (7) and (11)–(13) reveal a set of parameters that determine the dynamics of the evolution of the scattering process. It is necessary to distinguish between two groups of parameters of different importance. Obviously, the intensity $\hat{I}$ of the incoming laser flux, the equilibrium density n_0, the profile length L, and the coefficients causing dissipation ν, μ,

$$\{\hat{I},n_0,L,\nu,\mu\}$$

have direct influence on the dynamics of SBS. On the other hand, the Debye screening, causing dispersion in the case of $k_d\lambda_D > 0$, as well as the frequency ratio ω_d/ω_0 only become decisive in extreme situations of SBS in plasmas. The parameters applied in the calculations correspond to intensities up to $10^{13},\ldots,10^{16}$ W cm^{-2} (for Nd lasers) in plasmas with electron temperatures between 500 eV and 5 keV [e.g., $\hat{I}=0.8$ corresponds, according to Eq. (13), to 10^{16} W cm^{-2} with 5 keV, or 10^{15} W cm^{-2} with 500 eV], and homogeneous profiles up to 160 acoustic wavelengths ($\approx$80 em wavelengths). The used values for the coefficient $\mu(\sim T_i/\nu_{11}\sim T_i^{5/2};\ \mu k_d^2/\omega_d\approx 0.05,\ldots,0.3)$ have been computed from Braginskii's formulas in Ref. 18 considering heat conduction and viscosity corresponding to temperature ratios T_e/T_i below 100 for $Z=1$. We shall concentrate on the main set of parameters when discussing systematic changes in the numerical calculations. Before this (subject of Sec. IV), we examine the importance of those effects due to parameters that appear additionally in the context of this extended model. The main differences for the numerical treatment between the standard model with envelope equations and the extended model are displayed in Appendix D.

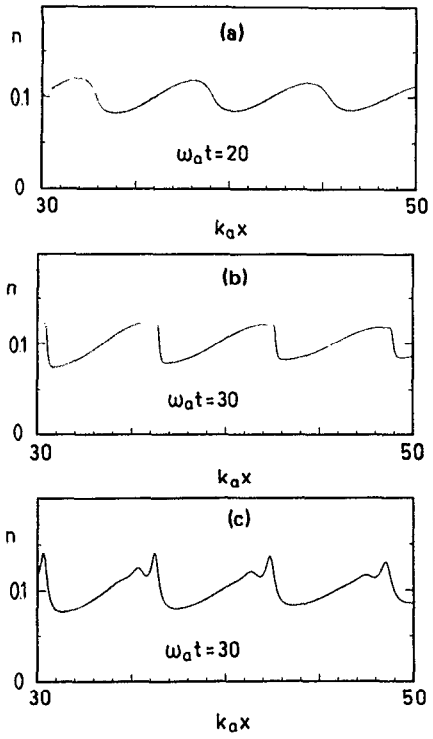

FIG. 2. Density perturbation of a sound wave in an early (a) and later stages (b) and (c) illustrating the nonlinear wave profile modifications during their propagation. At $\omega t = 30$ (b) without charge separation, $k\lambda_D = 0$, (c) with charge separation, $k\lambda_D \approx 0.1$ as a parameter in Poisson's equation.

B. Charge separation

The effect of charge separation causes dispersion of IAW's. It is illustrated in Fig. 2 by comparing a part an IAW profile in the case of $k_a\lambda_D = 0$ and $k_a\lambda_D = 0.1$. In both cases, an initially sinusoidal wave $v(x)$ deforms due to the different velocities of propagation dependent on the local amplitude. Without the action of any dissipative and dispersive processes, the wave profile becomes multivalued after the coordinates of two fluid elements overtake (in the sense of the hydrodynamic waterbag model[16]). When this occurs, the transformation from the Lagrangian to the Eulerian grid is no longer unique.[1,19] In the presence of friction, the discontinuities, which occur periodically for an initially periodic structure, are prevented ("shock fitting") by a jump in v over a finite interval of the width[3,14] $\delta = 2\mu/\Delta v$. The resulting periodic weak shock wave with the jump Δv in $v(x)$ from $x - \delta/2$ to $x + \delta/2$ exhibits a different structure when the mutual excitation of harmonics is more and more suppressed because of the mismatch

$$\Delta\omega_n \approx nsk_a[(1 + n^2k_a^2\lambda_D^2)^{-1} - 1]$$
$$\approx -n^3sk_a^3\lambda_D^2 \quad \text{for } (k_a\lambda_D)^2 \ll 1.$$

It is caused by the non-neutrality due to charge separation below scales of the Debye radius λ_D. Although the mismatch might be unimportant for the fundamental IAW, higher harmonics experience considerable dispersion, increasing strongly with the order of the harmonic "n." Then the spectrum of the IAW harmonics is cut off above $n > 1/(k_a\lambda_D)$ and thus structures with characteristic lengths $\delta \geqslant \lambda_D$ appear to be favored as is obvious from Fig. 2.

The latter effect has been studied in Ref. 9 in absence of a strongly k-dependent damping of the IAW due to viscosity. We will refer to weakly damped, but dispersive IAW's in Sec. IV since they are inseparably connected with kinetic processes of the ions.

However, the influence of dispersion due to charge separation, i.e., whether $0 < (k_a\lambda_D)^2 \ll 1$ or $k_a\lambda_D = 0$, is insignificant for the scattering as long as lower harmonics ($m \leqslant 3$) are not affected by a considerable spectral shift. From the computational point of view, the case $k_a\lambda_D = 0$ avoids the solution of Poisson's equation since the potential ϕ is simply given by

$$\Phi = \Phi_p + \ln(n_e/n_0) \tag{12'}$$

with $n_e|_{x_a} = Zn_a$. If $k_a\lambda_D \neq 0$, the nonlinear equation (12) has to be solved with the help of an iterative procedure[17] by setting $\exp(\Phi^{(i)}) \approx \exp(\Phi^{(i-1)}) \cdot (1 + \Phi^{(i)} - \Phi^{(i-1)})$, and repeating the integration $i = 1,...,3$ times to achieve good convergence. On the other hand, the boundary conditions, which become necessary in this case, may be advantageous since an undesired expansion of the profile can be suppressed. For the region left of the boundary $x = 0$, where the laser (pump) wave enters the plasma from $x = -\infty$, the electron density should remain, $n_e = 0$, and the condition

$$\left.\frac{\partial^2\Phi}{\partial x^2}\right|_{x_a<0} = (k_a\lambda_D)^{-2}(-Zn_i/n_0) = 0, \tag{14a}$$

together with $\partial_x\Phi(x < 0) = \partial_x\Phi_p(x < 0)$ is used. The same condition is possible for $x > L$, where L denotes the total length of the profile including the ramps, but we preferred setting

$$\left.\frac{\partial^2\Phi}{\partial x^2}\right|_{x_a>L} = 0, \tag{14b}$$

which means $n_e(x > L) = Zn_i(x > L)$, and which is reasonable as long as no counterpropagating light wave enters from the right.

C. The electromagnetic wave

The parameter ω_a/ω_0, which only appears in the em wave equation (7), influences the character of this quasilinear differential equation. For $\omega_a/\omega_0 \to 0$, the resulting ordinary differential equation physically describes the em field E as following the dynamics of the ion fluid instantaneously without memory, as in an already-established steady state.

In the case of nonstationary solutions and during the initial SBS instability, starting from tiny perturbations of the equilibrium, Eq. (7) has to be solved as a partial differential equation ($\omega_a/\omega_0 \neq 0$). We examined the time evolution by solving both the case $\omega_a/\omega_0 = 0$ with the help of the NAG Adams routine[20] D02CBF, and the case $0 < \omega_a/\omega_0 \ll 1$ using a Crank–Nicolson scheme. Since the ac-

curacy of the spatial integration by the Adams routine was only insignificantly better, we preferred the implicit Crank–Nicolson scheme because of the higher efficiency in computation time. In most of the numerical calculations, we used the same value $\omega_a/\omega_0 = 1/400$, which is already remarkably high for laser plasmas, but differences with lower values as well as $\omega_a/\omega_0 = 0$ proved to be insignificant.

At the boundary $x = 0$, it is reasonable to assume E to be composed of an incoming "pump" wave of fixed amplitude $\hat{E}$ and a reflected or backscattered wave E_1, both with almost equal wave vectors $\mathbf{k}_0$ and $\mathbf{k}_1$ of opposite sign, $\mathbf{k}_1 \approx -\mathbf{k}_0 = (\omega_0/c)\mathbf{e}_x$. The condition at $x = 0$ using $E(x = 0) = \hat{E} + E_1(x = 0)$ results, after normalization of the spatial coordinate with k_a, in the expression

$$\left.\frac{\partial E}{\partial x}\right|_{x=0} = i\frac{\omega_0}{c}\frac{1}{k_a}(2\hat{E} - E|_{x=0}). \tag{15a}$$

At the opposite boundary $x = L$, we exclusively considered the usual case of partial transmission of the pump wave [with wave vector $\mathbf{k}_0 = (\omega_0/c)\mathbf{e}_x$]

$$\left.\frac{\partial E}{\partial x}\right|_{x=L} = i\frac{\omega_0}{c}\frac{1}{k_a}E\Big|_{x=L} \tag{15b}$$

and neither any counterpropagating component from $x = \infty$ nor a reflective boundary. However, the shape of the equilibrium density profile causes tiny amplitudes of a counterpropagating wave inside the plasma. This can only insignificantly contribute to the value of the backscattered or reflected wave amplitude at $x = 0$, which is defined by

$$|E_1| = R^{1/2}\hat{E}$$

with

$$R = |[E(x=0,t)/\hat{E}] - 1|^2. \tag{16}$$

D. Initial conditions

When SBS evolves, the eventually dominant IAW mode has to grow up out of the competition with all other IAW modes in white thermal noise. In order to avoid a delay caused by this competition in the calculations, we superpose a coherent initial perturbation of the expected dominant mode on the equilibrium density profile by applying a small driving electrostatic field on the fluid. This method is equivalent to the assumption of an initial IAW amplitude perturbation in the usual coupled wave envelope theory.

Since the instability saturates because of nonlinear effects, the eventual state must be independent of the initial perturbation unless the solution is nonstationary and is sensitive to any phase shift. But the latter case cannot be observed together with the boundary conditions applied because of the geometry investigated here; nevertheless, a divergent evolution of solutions with closely neighbored initial conditions is a decisive point in the understanding of real situations in (inhomogeneous) laser plasmas.

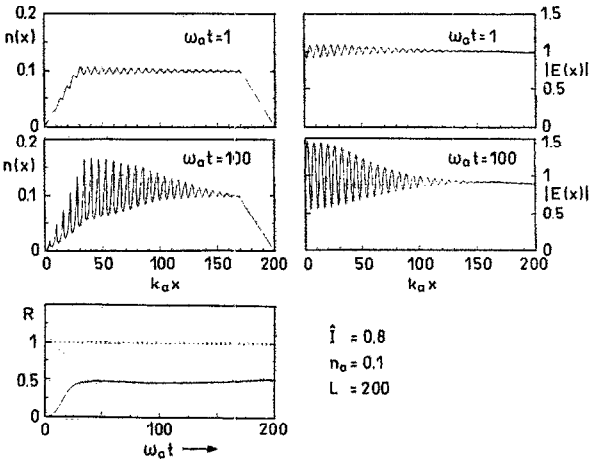

FIG. 3. Ion density and electromagnetic field amplitude in an early (a) and a later stage (b) of the SBS instability, in a trapezoidal profile corresponding to (a) $\omega t = 10$ and (b) $\omega t = 100$. (c) shows the temporal evolution of the backscattering level $R^{1/2}$ for the shown trapezoidal profile. Parameters: $\hat{I} = 0.8$, $n_0 = 0.1$, $L = 200$, $\nu_1 = 0.12$ ($\nu = 0.02$, $\mu = 0.2$), $\omega_0/\omega_a = 1000$.

E. Evolution and final state

The details of the initial SBS instability and its threshold—which is usually extremely low for SBS—can be described sufficiently by the usual linearized theory. Therefore our interest concentrates on the nonlinear evolution and the particular parameter dependence of the asymptotic steady state.

A typical temporal evolution of the backscattering amplitude, as well as the spatial profiles of the density and the em field in an early and a later stage, are shown in Fig. 3. The high-density perturbations of the IAW exhibit strong nonlinear deformation as shown enlarged in Fig. 2. Recognize that the oscillations in x of the em field amplitude $|E|$ are a consequence of the superposition of the counterpropagating wave contributions. The envelope of the oscillation amplitudes exhibits the local level of backscattering.

As long as the pump wave is not depleted, the amplitude of the backscattered wave grows during its passage through the IAW density perturbation. Its superposition with the incident wave causes a ponderomotive force acting on the fluid, even in absence of already existing considerable IAW levels (e.g., the region left of $x = 30$). Hence the SBS process comes up everywhere, even in the ramp of the considered trapezoidal profile on which the incident laser impinges, but less in the density ramp on the right (where the light does not enter). The latter effect, which has also been observed by Forslund *et al.* in Ref. 13, occurs independently of the depletion of the incident wave at the rear side of the profile.

Nonetheless, pump depletion is the main nonlinear effect that saturates the SBS instability. The saturation process and the pump depletion are consequences of the finite number of quanta (photons and phonons) that can be exchanged between the interacting modes and the flux of quanta that are dissipated irreversibly.

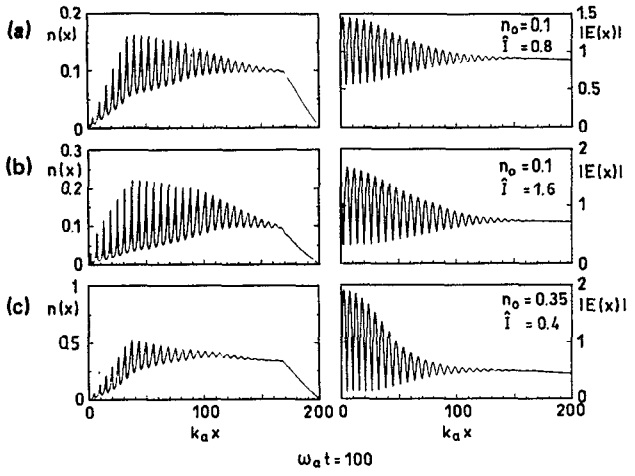

FIG. 4. Ion density and electromagnetic field amplitude as in Fig. 3 after the onset of an almost steady state for different parameters, (a) $\hat{I} = 0.8$, $n_0 = 0.1$, (b) $\hat{I} = 1.6$, $n_0 = 0.1$, (c) $\hat{I} = 0.4$, $n_0 = 0.35$. Further parameters: $L = 200$, $\nu_1 = 0.12$ ($\nu = 0.02, \mu = 0.2$), $\omega_0/\omega_a = 1000$.

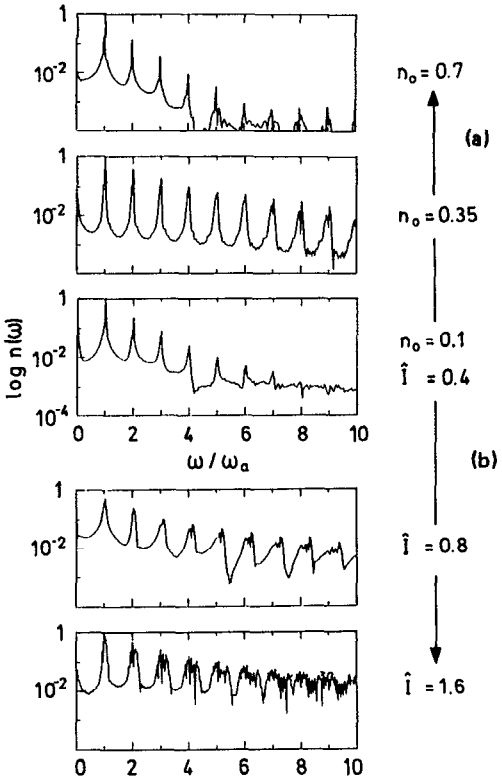

FIG. 5. Spectra of the ion acoustic waves for the parameters $L = 200$, $\nu_1 = 0.12$, $\omega_0/\omega_a = 1000$. In branch (a), the equilibrium density of the homogeneous profile is varied: $n_0 = 0.1, 0.35, 0.7$, whereas in branch (b), the intensity is increased $\hat{I} = 0.4, 0.8, 1.6$.

The nonlinear evolution of the IAW involves many more modes (i.e., harmonics) in the interaction process than the single IAW mode, which is usually assumed to contribute to stimulated scattering of em waves. When the exchanging flux between the harmonics and the dissipative flux proceeds to equilibrate, the backscattering will be diminished compared with the ordinary (or pure) SBS process without any IAW nonlinearities. The length of time before the equilibrium will be attained is mainly determined by the mutual coupling. This is dependent on external parameters, such as the intensity and the temperature, which determines the damping of the different wave components. However, as is obvious from Eq. (9) and Fig. 1, one has to distinguish between two different coupling circuits, one describing the interaction between the fundamental IAW and the ponderomotive force of the em waves, and another including the rather complex exchange between the harmonics of the IAW. After saturation of the SBS instability and after the onset of equilibrium, a final steady state appears which exhibits a constant level of backscattering in time.

IV. PARAMETER SCALING

A. Numerical results

As a result of numerous numerical calculations, we find the scaling of the parameters that determine the value of the backscattered light flux R observed at the location $x = 0$, where the incident light enters the plasma profile. Examples of variations in parameters in single calculations are presented in Figs. 4 and 5, which show snapshots of spatial profiles and the corresponding IAW and em wave spectra. As can be seen from Fig. 3, the envelopes (!) of the em wave and the IAW are slowly varying in x and are purely aperiodic. The observable spatial amplification of the backscattering from the rear to the front side of the plasma profile are typical solutions for the case of sufficiently damped IAW's.[12,21] Other types of solutions cannot be observed because they are less stable.

A parameter dependence summary is given in Fig. 6. The boundary condition for the electromagnetic wave is chosen according to Eq. (15b). The edges in the density ramps cause a small reflection.[22] This seeds the SBS process at an intensity of 5×10^{-6} related to the incident light flux at the rear side of the profile, $x = L$. The scaling of the abscissa in Fig. 6 was chosen in such a way that all curves should merge into the single one that appears in the case of a purely linear IAW according to the particular spatially aperiodic solution.[12] In order to see the actual features of SBS in presence of nonlinear IAW's, it was also necessary to reproduce also the behavior of the linearized case fitted to the considered trapezoidal profile. This is achieved by suppressing the higher-harmonic IAW modes. Both parameters $\hat{I}$ and n_0 were changed simultaneously whereas their product remained constant. This mainly causes a change in the refractive index $\eta = (1 - n_0/n_c)^{1/2}$, which has almost no influence on harmonic excitation, but which changes the decisive gain parameter G for spatial amplification.

As a result of our numerical calculations, we can conclude that the backscattering generally grows less fast as a function of any of the parameters than expected from the theory assuming a linearized IAW. The growth due to spatial amplification, when changing only the incident light intensity $\sim\hat{I}$ by a factor Λ, proves to be the least pro-

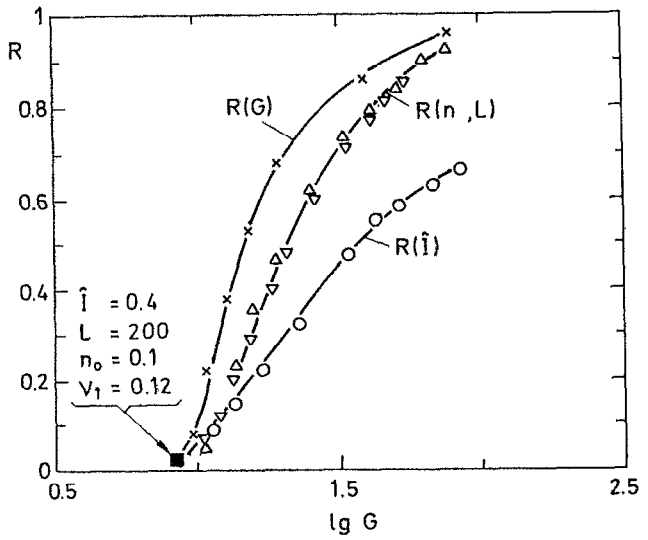

FIG. 6. Temporally asymptotic values of the backscattered light flux R at the transition to the vacuum ($x = 0$) determined from numerous calculations as a function of different parameters as indicated by the symbols. ∇: $R = R(L)$, Δ: $R = R(n_0)$, $\circ$: $R = R(\hat{I})$, and each other parameter fixed, $\times$: case of a linearized IAW $R = R(G)$. Starting from the indicated point, each increment of a single parameter is equally scaled corresponding to the values of the gain parameter G on the axes.

nounced. However, any change by Λ in either the profile length L or n_0/η (keeping $\hat{I}$ constant) causes an equivalent increment in R as a function of their product n_0L/η. That is,

$$R\left(\Lambda L, \frac{n_0}{\eta}, \hat{I}\right) = R\left(L, \frac{\Lambda n_0}{\eta}, \hat{I}\right) > R\left(L, \frac{n_0}{\eta}, \Lambda\hat{I}\right) \quad \text{for } \Lambda > 1,$$

where the product n_0L/η remains a similarity parameter, i.e.,

$$R(n_0/\eta, L) = R(n_0L/\eta),$$

as in the theory for a linearized IAW, where the product $(\hat{I}/\nu_1)\cdot n_0L/\eta \sim G$ determines the parameter scaling of R. It is physically apparent that the profile length or the equilibrium density are noncritical quantities from the viewpoint of harmonic excitation, as long as frictional damping is non-negligible, and thus the original scaling law is unaffected by any change of these parameters.

The resulting scaling of the parameters $\hat{I}$, n_0, and L leads to the apparent conclusion that none of those nonlinear analytic steady solutions[5,6] satisfy the considered physical situation. In the analytic solutions, only the dissipation of the fundamental IAW due to harmonic excitation is considered and no dissipation by friction causes the saturation of the scattering. These all are restricted to the case of weakly damped IAW's when the frictional terms become totally negligible compared with nonlinear dissipation. We shall see later that this case cannot be treated as decoupled from the onset of considerable kinetic effects, namely wave–particle interaction.

B. Analytical approach

In the following, we show that the same scaling is also a result of an analytic model using the conventional system of envelope equations for the em waves and a set of IAW harmonics, which all are sufficiently damped, making the convection of their energy negligible.

The assumption that the damping of each IAW harmonic is sufficiently large, which allows one to neglect the spatial derivative of the respective envelopes, is justified by the increase due to the k-dependent dissipation $\nu_n = \nu(nk)$. Even for the fundamental wave, this usually is reasonable, and therefore we will disregard all terms $\partial_x w_n$ in the steady-state limit of Eq. (9), i.e., $\partial_t w_n = 0$. The resulting system of nonlinear equations,

$$\nu_n w_n = \frac{1}{2}\varphi_p\delta_{1,n} - \frac{n}{2}\left(\sum_{m<n} w_m w_{n-m} - 2\sum_m w_m w_{m+n}\right), \tag{17}$$

can be iteratively solved by assuming that all harmonics $w_{n>1}$ are determined by the fundamental w_1, which is the only harmonic that couples to an external process, i.e., the ponderomotive force due to SBS. This procedure may be justified by the fact that all Eqs. (17) are homogeneous except the one for $n = 1$. When we then assume that all harmonics can be expressed by a series expansion in w_1, we find

$$w_1 = \frac{1}{2\nu_1}\varphi_p + w_1 P(w_1) = \frac{\varphi_p/(2\nu_1)}{1 - P(w_1)}, \tag{18}$$

with

$$P(w_1) = \frac{1}{\nu_1}\left(w_2(w_1) + \frac{1}{w_1}\sum_n w_n(w_1)w_{n+1}(w_1)\right). \tag{19}$$

In practice, a representation of P as a rapidly converging expansion of w_1 can be achieved using Padé's summation approximation with continued fractions. The coefficients of $P(w_1)$ depend on the damping factors $\nu_n = \nu(nk)$. Since we search for a solution of w_1 that guarantees the transition to the linearized case $w_{n>1} = 0$, $P(w_1)$ can be successively expanded around $w_1^{(0)} = \hat{w} = (1/2\nu_1)\varphi_p$. This finally yields

$$w_1 = w_1^{(\infty)} = \hat{w}\cdot[1/(1 - P^{\infty})]. \tag{20}$$

Here, the function $P^{\infty}(\hat{w})$, which now depends on the external parameter $\hat{w}$, replaces $P(w_1)$ and is asymptotically determined from the recursive iteration $P^{(i)}(\hat{w})$ that starts with $P^{(1)}(\hat{w}) = P(\hat{w})$. For details of the procedure, we refer to Appendix B.

In order to determine the steady-state solution of the backscattering process, the em field in Eq. (7) can be split, as usual, into two counterpropagating contributions, representing the incoming "pump" wave e_0 and the backscattered wave e_1. Since we want to concentrate on the problem of parameter scaling, we restrict ourselves to the case of a

homogeneous plasma slab and the assumption of ideal SBS matching, resulting in

$$v_{gr}\frac{\partial e_0}{\partial x} = -n_0\frac{\omega_0}{4}w_1 e_1, \tag{21a}$$

$$v_{gr}\frac{\partial e_1}{\partial x} = -n_0\frac{\omega_1}{4}w_1 e_0. \tag{21b}$$

Here, e_0, e_1, and w_1, are pure real-valued quantities, $v_{gr} = c\eta$ is the group velocity, and n_0, normalized to n_c, is the equilibrium density. We can assume that ω_0 and ω_1 are almost equal. Hence the square amplitudes $I_0 = e_0^2$ and $I_1 = e_1^2$ experience the same differential decrement

$$\frac{dI_0}{dx} = \frac{dI_1}{dx} = -\frac{\omega_0}{2v_{gr}}e_0 e_1 w_1 \sim \left\langle v(x)\frac{\partial \Phi_p}{\partial x}\right\rangle, \tag{22}$$

proportional to the correlation of the coupling between IAW and ponderomotive force. With the use of Eq. (20), we can eliminate w_1 in Eq. (22). In Eq. (20), φ_p stands for the oscillation amplitude of the ponderomotive force. In this notation it assumes the form $\varphi_p = \hat{I}\cdot e_0 e_1$. Since the photon number is conserved,

$$I_0 - \frac{\omega_0}{\omega_1}I_1 \approx I_0 - I_1 = (1-R)\hat{I} = \text{const}, \tag{23}$$

the spatial amplification of SBS is a result of the following integral using the boundary values $I_1(L) = \alpha^2$ and $I_1(0) = R$, with $I_0(0) = 1$:

$$\int_{\alpha^2}^{R}\frac{1 - P^{\infty}(I_0 I_1)}{I_0 I_1}dI_1 = -\int_L^0 n_0\frac{\omega_0}{4v_{gr}}\frac{\hat{I}}{\nu_1}dx = G. \tag{24a}$$

Here, α denotes the mean level of the backscattered wave due to thermal noise. Disregarding the function $P^{\infty}(\hat{w})$, Eq. (24) is the well-known integral of the aperiodic spatial amplification based on a linearized IAW,[10-12]

$$\int_{\alpha^2}^{R}\frac{dI}{I(I+1-R)} = \frac{1}{1-R}\ln\left(\frac{R(1-R)}{\alpha^2} + R\right) = G. \tag{24b}$$

The external parameters $\hat{I}$, n_0, ω_0/v_{gr}, and the profile length L then appear only on the rhs combined in a simple scaling: $G = (\omega_0 L/4c)(n_0/\eta) \times (\hat{I}/\nu_1)$. This scaling is now spoiled since $\hat{I}$ and the damping coefficients ν_n also appear in P^{∞}. However, it turns out that the scaling of n_0/η and L, resulting in their product $n_0 L/\eta$, remains unaffected and is still the same as obtained from the numerical data. The presence of IAW nonlinearities causes energy to be transferred from the fundamental into its harmonics. Therefore the function P^{∞} diminishes the spatial amplification of the backscattering. Its inclusion also requires that the gain parameter G must assume a larger value in order to achieve the same backscattering level R at $x = 0$ as in the presence of a pure linear IAW. Similar to Fig. 6, Fig. 7 shows the influence of this effect. Here, we compare the analytic solution of $R(G)$ in the case of an assumed linearized IAW with the solutions in the presence of nonlinear IAW's. Because of the different scaling, now two curves result: one when solely the parameter $n_0 L/\eta$ is varied, the other when only the intensity $\hat{I}$ is increased continuously. Both curves (dashed and dotted) shown in Fig. 7 correspond to the solution based on the first approximation $P^{(1)}(\hat{w})$ of the function $P^{\infty}(\hat{w})$ when one takes into account only products $w_m w_n$ up to the order $m + n < 4$, i.e.,

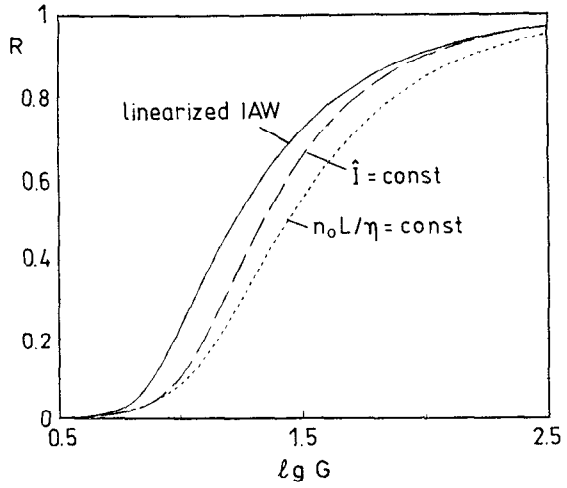

FIG. 7. Backscattered light flux values R obtained from the analytic steady-state solutions. The solid curve shows the behavior for a linearized IAW. Both of the other curves represent the simplest approximation for a nonlinear IAW by varying the laser flux I (dashed curve) for $n_0 L/\eta = 17$, and the similarity parameter $n_0 L/\eta$ (chain-dashed curve) for $\hat{I} = 0.4$. Further parameters: $\nu = 0.02$ and $\mu = 0.2$, and backscattering noise level $\alpha = 0.01$.

$$\begin{aligned} \nu_1 w_1 &= (\hat{I}/2)e_0 e_1 + w_1 w_2, \\ \nu_2 w_2 &= -w_1^2 + 2w_1 w_3, \\ \nu_3 w_3 &= -3w_1 w_2, \end{aligned} \tag{25}$$

using $\varphi_p = I\cdot e_0 e_1$. In a first approximation, one assumes $w_1 = \hat{w}\cdot[1 - P^{(1)}(\hat{w})]^{-1}$ and $P^{(1)}(\hat{w}) = P(\hat{w})$. This yields

$$P^{(1)}(\hat{w}) = P(\hat{w}) = -\frac{w_1^2/(\nu_1\nu_2)}{1 + 6w_1^2/(\nu_2\nu_3)} = -\frac{S_1 I_0 I_1}{1 + S_2 I_0 I_1}, \tag{26}$$

using $S_1 = \hat{I}^2/(4\nu_1^2\nu_2)$ and $S_2 = 3\hat{I}^2/(2\nu_1^2\nu_2\nu_3)$.

The function obtained above enables the evaluation of the integral equation (24) in this approximation, for which the solution yields an implicit and transcendental dependence in R on $\hat{I}$. We refer to Appendix C for the presentation of this particular approximation. Figure 7 shows the result corresponding to the usage of Eq. (26). A better approximation would result in a slightly different behavior of R as a function of the external parameters, but would obey the same scaling properties. We observe in Figs. 6 and 7 that both curves $R(n_0 L/\eta)$ and $R(\hat{I})$ merge into the case of a linearized IAW for $G + \ln\alpha^2 \ll 1$ or equivalently $\alpha^2 < R \ll 1$. Both remain below the solution for a linearized IAW, $R(G)$, beyond this range of small amplification. According to the analytic approximation, all three solutions do not saturate below $R = 1$, but approach this level with

delay in the gain parameter G. The same can be concluded from the values obtained analytically, except for the high-intensity regime where $R(\hat{I})$ clearly tends to remain below $R = 1$. For very high intensities, the analytic approximation fails since the nonlinear terms in Eq. (17) can no longer be compensated by only the damping terms. In this case, the spatial derivative of the IAW amplitudes in Eqs. (17) or (25) have to be included.

It is worthwhile to emphasize that the scaling of the backscattering due to our assumption of sufficiently damped IAW's is not restricted to a particular k dependence of $\nu_n = \nu(nk)$ as long as ν_1 already fulfills the assumptions $\nu_1 w_1 \gg s\,\partial_x w_1$ [we always used $\nu_n = \nu + (\mu/2)n^2k^2$ and ν was chosen as the Landau damping ν_L on the fundamental IAW[23]]. Scaling due to a balance of certain nonlinear terms in the harmonic, as obtained in Refs. 5 and 6, proved to be unsuitable to the results of our numerical scheme.

In our numerical calculations, we tried to examine the onset of the transition into the regime of less-damped IAW's. This is shown in Fig. 8, where R saturates and the type of the solution (see Ref. 12) changes to nonlinear trigonometric (Jacobi-elliptic) functions. These solutions are independent of damping and noise level α, which plays a role in the solution of aperiodic spatial amplification. The influence of IAW nonlinearities on this type of solutions has recently been investigated by Candy *et al.* (Ref. 9). It is questionable whether weakly damped IAW's can be treated when one disregards the onset of kinetic effects,

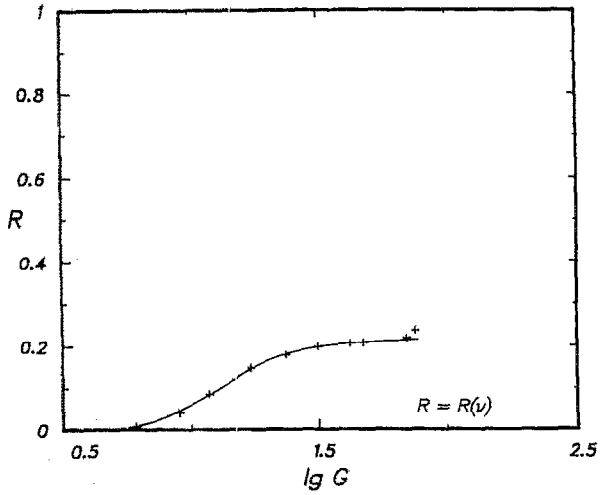

FIG. 8. Backscattered flux R as a function of the gain parameter by varying the damping ν_1 of the fundamental wave for $L = 200$, $n_0 = 0.1$, and $\hat{I} = 0.8$.

which invalidates the assumption of a simple ion velocity distribution in phase space, as is used for the hydrodynamic description. A discussion of this problem is the subject of the following section.

V. KINETIC EFFECTS

In order to examine the role of kinetic effects in the presence of SBS, we performed particle simulations of the

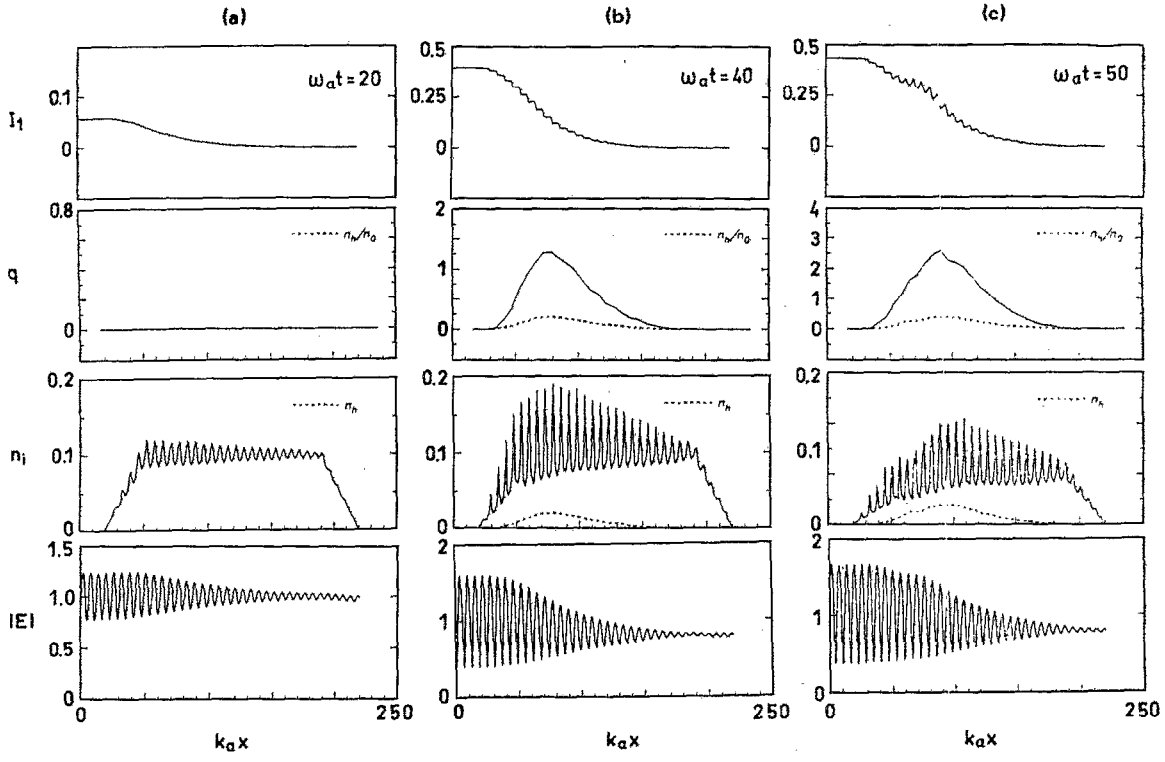

FIG. 9. Local backscattered flux $I_1(x)$, heat flux of the ions $q \sim \int v^3 f(v)dv$, ion density n, and electromagnetic field amplitude before (a) and after (b) and (c) the onset of anomalous heat transport due to trapped particles. The density of particles with a speed above the phase velocity of the wave, $n_h(v > u)$, is indicated by the dashed lines. Particle simulation with the parameters $L = 200$, $n_0 = 0.1$, $T_i/T_e = 0.02$ (initially), and $\hat{I} = 0.4$.

ions instead of solving their hydrodynamic equations. In Ref. 13, the high-frequency oscillations of the electrons were also treated by using a particle code for both the electron and ion species. In the more compact model investigated here, electrons are still assumed to form an isothermal background, so that, in the set of Eqs. (11) to (13), only (11) is replaced by

$$\frac{\partial v_\alpha}{\partial t} = -\left.\frac{\partial \Phi}{\partial x}\right|_{x_\alpha} \quad \text{and} \quad \frac{\partial x_\alpha}{\partial t} = v_\alpha . \tag{27}$$

Similar models were investigated in previous publications,[24] but in absence of a driving ponderomotive force due to SBS. In the 1-D particle code, up to 50 000 "particles" of size comparable to λ_D were used. Equation (27) does not include any dissipation due to external effects, and also no ion–ion collisions are included so that thermalization is not considered.[25] However, we ensured that the corresponding times due to ion–ion encounters and the times in which ion–electron collisions show influence on the ions were longer than the typical time of a run (i.e., $\omega_a t < 60$). (For $T_e/T_i \approx 50$ and $T_e \approx 2$ keV this is approximately the time in which a collision should occur.)

From the simulations, we observe that in an early stage, when the dynamic process of the instability growth is still active, the ion motion behaves as in the hydrodynamic case. This changes after some interval, resulting in strong "anomalous" heat transport that does not correspond to an irreversible thermal equilibration process, but to wave–particle interaction. Both stages are illustrated in Fig. 9. Strong wave–particle interaction occurs mainly close to the shock fronts of the successive IAW potential barriers where the potential jumps almost from $-\Phi$ to Φ, $\delta\Phi \approx 2\Phi$. Particles that move with respect to the IAW frame will be reflected off the potential walls from $v < v_\varphi$ to $v > v_\varphi$ or vice versa when their relative energy is too low, i.e., $(1/2)(v - v_\varphi)^2 < 2\Phi$. Here, $v_\varphi = \omega/k$ denotes the phase speed of the IAW. As long as the width of the velocity distributions of the ions (centered around $v = 0$) is small (i.e., "cold ions"), strong wave–particle interaction will only appear for wave amplitudes $v[\approx u^2(k/\omega)\Phi]$ above $v_\varphi - 2\Phi^{1/2}$. This results in $\Phi > 1 - 2\Phi^{1/2}$ or $\Phi > 0.17$, since sound and phase velocity are almost equal ($u \approx v_\varphi$) for IAW's. Because of this symmetry of the reflection of particles at walls moving with speed u, a jet of ions with a velocity of up to $2u$ can form, which succesively results in phase space mixing.

The IAW shock fronts can show structure due to dispersion as discussed in Sec. IV B and in Ref. 9, and the wave–particle interaction may be affected by the finite transition width. The dominant process, however, that influences the SBS process will be the following: "Anomalous" heat transport is caused by fast ions, that have been accelerated up to twice that of the sound velocity, $v_\alpha < 2v_\varphi \approx 2u$, by the potential barriers, as seen in the phase space plots in Fig. 10. The spatial amplification of backscattering is considerably reduced, as shown Figs. 9 and 11, due to the fact that fast ions do not contribute to the collective oscillatory motion of ions in the IAW field. The correlation

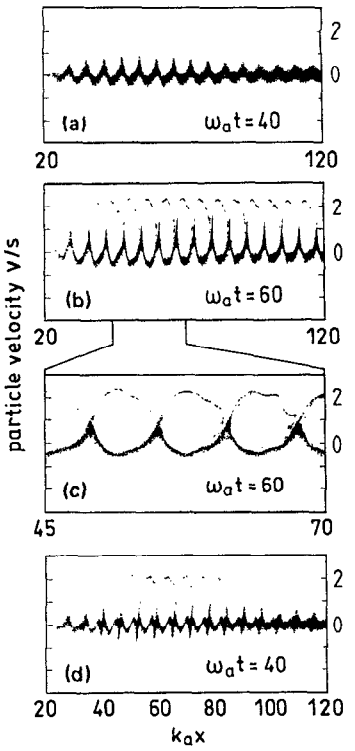

FIG. 10. Phase space snapshots showing all ions of particle simulations in the indicated intervals of x with an initial temperature ratio of $T_i/T_e = 0.02$. (a) Time $\omega t = 20$ and $\hat{I} = 0.4$, (b) $\omega t = 20$ and $\hat{I} = 1.6$, (c) as in (a) at $\omega t = 40$ shown enlarged in a smaller interval in (d). (a), (c), and (d) correspond to Fig. 9.

between the ion (electrostatic) wave field $v(x)$ and the ponderomotive force caused by SBS, namely [see Eqs. (10) and (22)]

$$\frac{\partial I_1}{\partial x} \sim \frac{1}{\lambda_a} \int_x^{x+\lambda_a} v(x') \frac{\partial \Phi_p}{\partial x} dx' = \left\langle v \frac{\partial \Phi_p}{\partial x} \right\rangle , \tag{28}$$

is diminished because of the reduced number of harmonically oscillating ions. The backscattered wave intensity

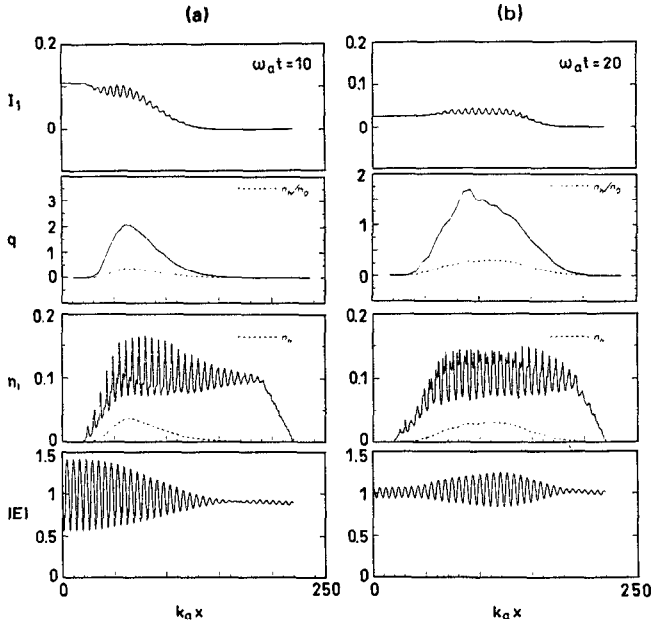

FIG. 11. As in Fig. 9, but with the initial temperature $T_i/T_e = 0.1$ and the laser intensity $\hat{I} = 1.6$, showing structures sometimes called "x-type" wave breaking. Figure 11 corresponds to the situation in Fig. 10(b).

I_1, illustrated in Figs. 9 and 11, has been calculated by integrating in space over successive IAW periods of $\partial_x \Phi_p$. The fluctuations in I_1 clearly correspond to the presence of anomalous heat flux due to fast ions. Their mean velocity $v_h = \int_{v>u} v f(v,x) dv / n_h > u$ [using the number density $n_h = \int_{v>u} f(v,x) dv$] is almost constant in x and yields oscillations when evaluating the integral

$$\int_x^{x+x_0} v_h \frac{\partial \Phi_p}{\partial x} dx' \approx v_h [\Phi_p(x+x_0) - \Phi_p(x)]. \quad (29)$$

These oscillations cancel out over an entire wave period λ_a because Φ_p is almost periodic, i.e., $\Phi_p(x + \lambda_a) = \Phi_p(x)$.

Of course, considerable ion or electron heat flux is also accompanied by a dc current and an ambipolar field in order to satisfy charge conservation. This results in an additional flow as indicated by Eq. (4) for Poisson's equation, in order to balance the electrostatic field of escaping electrons and ions, and also in a spatial temperature dependence. However, this does not strongly influence the considerations concerning the spatial amplification of SBS over subsequent periods of the IAW.

In previous publications, e.g., by Kruer *et al.* in Ref. 26, models estimating the compensation of laser flux, backscattered flux, and heat transport were introduced to determine qualitatively a mean level of SBS. On the other hand, the onset of an eventual, almost time-independent backscattering level strongly depends on the duration of the equilibration process connected with wave–particle interaction and heating of the ions in the plasma. This duration can be much longer than in cases that guarantee a sufficiently damped IAW's, and meanwhile, even high backscattering levels can occur.

VI. CONCLUSIONS AND DISCUSSION

We systematically investigated the influence of the inherent nonlinear properties of ion acoustic waves on SBS. We numerically solved an extended model using the hydrodynamic equations of the ion fluid as well as the electromagnetic wave equation. This set of equations is applied to almost homogeneous density profiles in order to enable a comparison with the usual theory.

The typical approach of SBS uses a linearized IAW. For sufficiently damped IAW's, it yields a simple scaling of the physically relevant parameters for the steady-state solutions with spatial amplification of the backscattering. This scaling no longer holds in the presence of IAW nonlinearities. The transition from the scaling with a single similarity parameter in the linearized case into several separate parameters becomes apparent for pronounced nonlinearities, particularly with increasing laser intensity. This is also reproduced using an analytic approach that involves ion wave harmonics. The resulting reduced backscattering compared with standard theory is similar to some experimental results with preformed homogeneous plasmas.[27] There, a strongly reduced increment in the backscattering level R as a function of the intensity without showing a saturation below $R = 1$ was observed.

The influence of IAW–particle interaction on SBS is also analyzed with the help of particle simulations. Such kinetic phenomena, as ion trapping and the accompanying anomalous heat transport, appear for weakly damped IAW's when the nonlinear shape of the wave affects the particle distribution function significantly. The IAW electrostatic field must be highly correlated to the ponderomotive force of the em wave in order to achieve an efficient scattering process. Therefore, a dc current due to fast particles weakens the amplification of the scattering process since only a reduced number of ions contribute to the field of the IAW. The subsequent phase space mixing may remain for a long time until the velocity distribution is in equilibrium with the dynamic processes. In contrast to the case of sufficiently damped IAW's, which can be expected for electron–ion temperature ratios $T_e/T_i < 50$ (considering also normal heat conduction and viscosity in the dissipation), this results in strongly nonstationary backscattering. Although the mean level of the backscattered signal will be lower than expected from the usual theory, intermediate values of $R(t)$ can still be considerably high.

ACKNOWLEDGMENTS

The author expresses his particular thanks to P. Mulser for enabling this work, for encouragement, and many stimulating discussions and to A. M. Rubenchik for his interest and many helpful remarks. The support by S. Coggeshall, and D. Jost-Gomes da Costa for carefully reading the manuscript and by J. Pfister for preparing the illustrations was a great help and is highly appreciated.

APPENDIX A: DERIVATION OF THE EQUATION FOR "QUASISIMPLE" WAVES

The same procedure as for a simple wave can be applied to Eqs. (2) when $\hat{\rho}^2 = (d\hat{\rho}/dv)^2 u^2$. Here, we used the definition for the normalized sound speed $u^2 = 1 + \gamma_i T_i/(Z T_e)$, and the additional condition that

$$\frac{d\psi}{dt} + u \frac{\partial \psi}{\partial x} = 0.$$

From Eqs. (2), we obtain the following differential equation for v:

$$\hat{\rho}\left(\frac{dv}{dt} + u\frac{\partial v}{\partial x}\right) = -\psi \frac{dv}{dt} - u\frac{\partial \psi}{\partial x} + \rho\left(\mu \frac{\partial v^2}{\partial x^2} - \frac{\partial \Phi_p}{\partial x}\right)$$

$$= -u\frac{\partial \psi}{\partial x} - \psi u \frac{\partial v}{\partial x}, \quad (A1)$$

where the deviations from Eq. (1) in absence of charge separation are of the same order of magnitude in ψ as the terms on the rhs of Eq. (2b) or of Eq. (A1). Using

$$\psi \frac{dv}{dt} \approx -\psi u \frac{\partial v}{\partial x} + \mathbf{O}(\psi^2),$$

we arrive at the equation for "quasisimple" waves, which is in second-order accurate in ψ,

$$\frac{\partial v}{\partial t}+[u(v)+v]\frac{\partial v}{\partial x}=\frac{1}{2}\left(\mu\frac{\partial^2 v}{\partial x^2}-\frac{\partial \Phi_p}{\partial x}\right)+\mathbf{O}(\psi^2). \tag{A2}$$

In the following, we shall determine the deviation from the original hydrodynamic equations (2). Therefore the expansion of the steady-state representation of Eqs. (2), derived in Ref. 28,

$$\left(M-\frac{1}{M}\right)\frac{\partial M}{\partial x}=-\frac{\partial \Phi_p}{\partial x}+\mu\frac{\partial^2 M}{\partial x^2}, \tag{A3}$$

reveals the leading term in powers of the velocity in the frame of the acoustic wave $v=M-1$. Here, M is defined as the Mach number of a flow assuming $T_i \ll T_e$ [$u(v)=1$],

$$v\frac{\partial v}{\partial x}-\frac{1}{2}\left(\mu\frac{\partial^2 v}{\partial x^2}-\frac{\partial \varphi_p}{\partial x}\right)-\frac{1}{2}\left(1-v-\frac{1}{1+v}\right)\frac{\partial v}{\partial x}$$

$$\approx -\frac{1}{2}(v^2-v^3+v^4-\cdots)\frac{\partial v}{\partial x}. \tag{A4}$$

The rhs in Eq. (A4) is an estimate for the error indicated above by $\mathbf{O}(\psi^2)$. The only nonlinearity in the "simple wave equation" Eq. (A2), $v\partial_x v$, balances the force terms. The next-order nonlinear contribution, $(1/2)v^2\partial_x v$, was disregarded and causes any harmonic expansion based on Eq. (A2) to become erroneous with increasing order. Recognize that, without any dissipative term, the case of a linear sound wave, $M=1$, Eq. (A3) cannot describe the situation adequately unless the ion inertia is included.

APPENDIX B: ITERATIVE DETERMINATION OF THE FUNDAMENTAL IAW AMPLITUDE

The inversion of Eq. (18),

$$w_1=w_1^{(\infty)}=\hat{w}[1/(1-P^{\infty})],$$

can be achieved iteratively by using a convergent expansion

$$w_1^{(i+1)}=\hat{w}\frac{1-[P'/(1-P^{(j)})]w_1^{(j)}}{1-P^{(j)}-[P'/(1-P^{(j)})]\hat{w}}$$

$$=\hat{w}\frac{1}{1-P^{(j+1)}} \tag{B1}$$

with j as the iteration step, $P^{(j)}(\hat{w})$ as the recursive function, and $P'=\partial P^{(j)}/\partial\hat{w}$. One starts with $P^{(1)}(\hat{w})=P(\hat{w})$. For large enough j, $P^{(j)}$ should converge, which implies $P^{\infty}\approx P^{(j+1)}\approx P^{(j)}$ and $w_1^{(j+1)}\approx w_1^{(j)}\approx w_1$.

APPENDIX C: INTEGRAL EVALUATION FOR REDUCED SPATIAL AMPLIFICATION

Using the approximation in Eq. (26b) to replace the function P in Eq. (24), the integral results in

$$\int_{\alpha^2}^{R}\left(\frac{dI_1}{I_0 I_1}+S_1\frac{dI_1}{1+S_2 I_0 I_1}\right)=G. \tag{C1}$$

The first term on the LHS, see Eq. (24a), is well known. With the photon flux conservation Eq. (22) one yields the second integral,

$$\int_{\alpha^2}^{R}\frac{dI}{1+SI(1-R+I)}=\begin{cases}\dfrac{2}{S\Lambda^{1/2}}\arctan\dfrac{2(\alpha^2-R)\Lambda^{1/2}}{\Lambda+(1+R)(1-R+2\alpha^2)}, & \Lambda>0,\\[2ex] \dfrac{1}{S(-\Lambda)^{1/2}}\ln\dfrac{[1-R+2\alpha^2-(-\Lambda)^{1/2}][1+R+(-\Lambda)^{1/2}]}{[1-R+2\alpha^2+(-\Lambda)^{1/2}][1+R-(-\Lambda)^{1/2}]}, & \Lambda<0,\end{cases} \tag{C2}$$

with $\Lambda=(4/S)-(1-R)^2$. It corresponds to the IAW nonlinearities and causes the spatial amplification for the gain parameter G to be less efficient.

APPENDIX D: COMPARISON OF NUMERICAL SCHEMES

TABLE I.

Standard system (envelope equations)	Extended model
Ion Acoustic Wave	
(a) Initial condition	
Density fluctuations due to thermal noise	
Small amplitude on thermal noise level	Small propagating perturbation in potential Φ or density n
(b) Boundary conditions	
Vanishing amplitude at $x=0$ (without importance for heavily damped IAW's)	Intrinsically given by the initial profile and the definition of the Lagrangian mesh, In case of charge separation additional conditions equations (14) for Poisson's equation
Electromagnetic Wave	
(a) Initial conditions	
For incident wave: Level of lasers pulse at $t=0$	Initial boundary conditions, equivalent to standard model

TABLE I. (*Continued.*)

Standard system (envelope equations)	Extended model
For backscattered wave: small amplitude on thermal noise level	together with integration over the initial profile
(b) Boundary conditions	
For incident wave: Laser pulse as a function of t at $x = 0$	Superposition of incident and backscattered wave at $x = 0$, Eq. (15a)
For backscattered wave: Noise level at the rear side $x = L$ or reflection	Transmitted light level at $x = L$, Eq. (15b), superposed by counterpropagating light wave (optional, not considered here).

[1] L. D. Landau and E. M. Lifshitz, *Course of Theoretical Physics* (Pergamon, London, 1959), Vol. 6.

[2] D. Mihalas and B. Weibel-Mihalas, *Foundations of Radiation Hydrodynamics* (Oxford U.P., Oxford, 1984).

[3] G. B. Whitham, *Linear and Nonlinear Waves* (Wiley, New York, 1974).

[4] S. Hüller, P. Mulser, and A. M. Rubenchik, Phys. Fluids B **3**, 3339 (1991); S. Hüller, P. Mulser, and H. Schnabl, in *Laser Interaction and Related Plasma Phenomena*, edited by H. Hora and G. H. Miley (Plenum, New York, 1991), Vol. 9.

[5] S. J. Karttunen and R. R. E. Salomaa, Phys. Lett. A **88**, 350 (1982); S. J. Karttunen, J. N. McMullin, and A. A. Offenberger, Phys. Fluids **24**, 447 (1981).

[6] V. P. Silin and V. T. Tikhonchuk, Sov. Phys. JETP **56**, 765 (1982).

[7] K. Baumgärtel and K. Sauer, *Topics on Nonlinear Wave–Plasma Interaction* (Birkhäuser, Basel, 1987), Chap. IV.

[8] M. Casanova, G. Laval, R. Pellat, and D. Pesme, Phys. Rev. Lett. **54**, 2230 (1985).

[9] J. Candy, W. Rozmus, and V. T. Tikhonchuk, Phys. Rev. Lett. **65**, 1889 (1990).

[10] C. L. Tang, J. Appl. Phys. **37**, 2945 (1966).

[11] W. L. Kruer, Phys. Fluids **23**, 1273 (1980).

[12] V. Fuchs, Phys. Fluids **19**, 1554 (1976).

[13] D. W. Forslund, J. M. Kindel, and E. L. Lindman, Phys. Fluids **18**, 1017 (1975).

[14] V. I. Karpmann, *Nonlinear Waves in Dispersive Media* (Pergamon, Oxford, 1984).

[15] In linearized theory, all daughter waves are suppressed; thus the sum is reduced to $m = 1$ and the rhs in Eq. (10) vanishes.

[16] R. C. Davidson, *Methods in Nonlinear Plasma Theory* (Academic, New York, 1972).

[17] Ch. Sack and H. Schamel, Phys. Rep. **156**, 311 (1987).

[18] S. I. Braginskii, *Transport Processes in Plasmas in Review of Plasma Physics*, edited by A. M. Leontovich (Consultants Bureau, New York, 1965), Vol. 1, Chap. IV.

[19] D. Montgomery, Phys. Rev. Lett. **19**, 1465 (1967).

[20] The Numerical Algorithms Group Ltd., *The NAG Fortran Library* (Oxford, 1987).

[21] R. W. Harvey and G. Schmidt, Phys. Fluids **18**, 1395 (1975).

[22] V. L. Ginzburg, *The Propagation of Electromagnetic Waves in Plasmas* (Pergamon, Oxford, 1964), Sec. 16.

[23] The k dependence of Landau damping, $\nu \sim nsk_a$, was not possible to simulate by simple means in the hydro equations without causing undesired dispersion. For the harmonics, therefore, the role of Landau damping was underestimated in the numerical calculations.

[24] D. W. Forslund, J. M. Kindel, and K. Lee, Phys. Fluids **22**, 462 (1979); W. E. Hobbs and J. S. de Groot, Phys. Fluids **20**, 1109 (1977).

[25] A direct comparison between the fluid and the particle calculations with identical parameters over a long time interval has to take into account also comparable dissipative processes. Lagrangian fluid codes always contain phenomenological damping like viscous terms that also represent thermal equilibration (heat conduction). On the other hand, in collisionless particle codes wave–particle interaction (causing Landau damping) is the only intrinsic dissipative mechanism. Therefore both numerical schemes cover different parameter regimes, particularly in the temperatures T_e and T_i.

[26] W. L. Kruer and K. Estabrook, in *Laser Interaction and Related Plasma Phenomena*, edited by H. Schwarz and H. Hora (Plenum, New York, 1980), Vol. 5.

[27] J. Handke, A. H. Rizvi, and B. Kronast, Appl. Phys. **25**, 109 (1981); B. Gellert and B. Kronast, Appl. Phys. **B33**, 29 (1984).

[28] P. Mulser and G. Spindler, Z. Naturforsch. **34a**, 1059 (1979).